Inorganic Chemistry

ARTICLE

pubs.acs.org/IC

Site-Preferential Design of Itinerant Ferromagnetic Borides: Experimental and Theoretical Investigation of MRh_6B_3 (M = Fe, Co)

Patrick R. N. Misse, Michael Gilleßen, and Boniface P. T. Fokwa*

Institute of Inorganic Chemistry, RWTH Aachen University, 52056 Aachen, Germany.

Supporting Information

ABSTRACT: Single-phase polycrystalline samples of the compounds MRh_6B_3 (M = Fe, Co) as well as single crystals of $CoRh_6B_3$ have been synthesized by arc-melting the elements under a purified argon atmosphere in a water-cooled copper crucible. The characterization of the new phases was achieved by using single-crystal and powder X-ray diffraction as well as EDX measurements. The two phases are isotypic and crystallize in the hexagonal Th_7Fe_3 structure type (space group $P6_3mc$, no. 186, $Z = 2$). In this structure, the magnetically active atoms (Fe, Co) are preferentially found on only one of the three available rhodium sites, and together with rhodium they build a three-dimensional network of interconnected $(Rh/M)_3$ triangles. Magnetic properties investigations show that both phases order ferromagnetically below Curie temperatures of 240 K (for $FeRh_6B_3$) and 150 K (for $CoRh_6B_3$). First-principles DFT calculations correctly reproduce not only the lattice parameters but also the ground state magnetic ordering in the two phases. These calculations also show that the long-range magnetic ordering in both phases occurs via indirect ferromagnetic coupling between the iron atoms mediated by rhodium. This magnetic structural model also predicts the saturation magnetizations to be 4.02 μ_B for $FeRh_6B_3$ (3.60 μ_B found experimentally) and 2.75 μ_B for $CoRh_6B_3$. Furthermore, both phases are predicted to be metallic conductors as expected for these intermetallic borides.

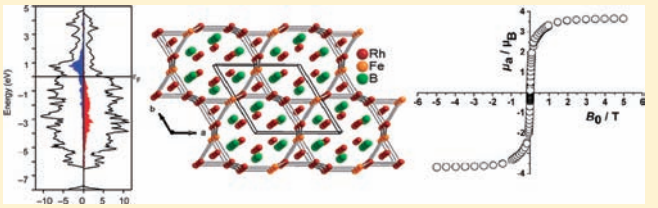

1. INTRODUCTION

In recent years, due to remarkable physical, chemical, and mechanical properties such as high melting points, excellent mechanical hardness, and itinerant magnetic properties, transition metal borides have attracted much interest.[1]

The Th_7Fe_3 structure type[2] (space group $P6_3mc$) has gained some attention in the physics community, because of the exciting physical properties which originate from this noncentrosymmetric structure: For example, the hydrogenation of superconducting Th_7Fe_3 leads to ferromagnetic $Th_7Fe_3H_{30}$,[3] giant magnetoresistance (GMR) is found in Th_7Rh_3,[4] and ferromagnetic transition is observed at about 334 K in Gd_7Pd_3,[5] just to name a few. Although many transition metal borides have been reported, which also crystallize in this structure type, they did not attract much attention like their isotypic intermetallic counterparts. For example, only Ru_7B_3 has recently (2009) been studied by two research groups who simultaneously confirmed superconducting properties already discovered in the 1960s.[6] However, to the best of our knowledge, magnetic ordering has not been observed in this class of borides, although a few phases containing magnetically active transition metals have been reported some 30 years ago, e.g., $Co_{0.77}Re_{6.23}B_3$[7] and $Ni_{0.5}Re_{6.5}B_3$.[8] In recent years, we have been studying ternary boride phases adopting the aforementioned structure type, focusing primarily on their crystal chemistry. In fact, during these studies, we have observed a strong site preference when partly substituting either rhodium (in Rh_7B_3) or ruthenium (in Ru_7B_3) by a magnetically active element: In the resulting ternary rhodium-containing $FeRh_6B_3$,[9] iron was found (together with rhodium) at only one of the three available rhodium positions, whereas in $Fe_xRh_{7-x}B_3$ ($1 < x \leq 1.5$)[10] and in $M_{0.5}Ru_{6.5}B_3$ (M = Cr, Mn, Fe, Co, Ni),[11] the magnetically active elements were present in two of the three rhodium or ruthenium sites. We have also reported the magnetic properties of the $M_{0.5}Ru_{6.5}B_3$ (M = Cr, Mn, Co, Ni) phases, which were found to be either Pauli paramagnets (M = Cr, Co, Ni) or a normal paramagnet ($Mn_{0.5}Ru_{6.5}B_3$), and no hint of magnetic ordering down to 4 K was found.

In this work, we will focus our attention on the synthesis and characterization of single phase polycrystalline samples of the $FeRh_6B_3$ phase in order to thoroughly investigate its magnetic properties. Moreover, we will try to also synthesize single phase polycrystalline material and single crystals of the unknown "$CoRh_6B_3$" phase and investigate its crystal structure and magnetic properties, as well. Last, we will support our experimental findings (lattice parameters, ground state magnetic orderings, and magnetic moments) by first-principles calculations of the density functional theory (DFT) type.

2. EXPERIMENTAL SECTION

2.1. Synthesis and Characterization. The title phases were prepared by arc-melting the pelletized powders of the elemental

Received: June 25, 2011
Published: September 12, 2011

ACS Publications © 2011 American Chemical Society

dx.doi.org/10.1021/ic2013655 | *Inorg. Chem.* 2011, 50, 10303–10309

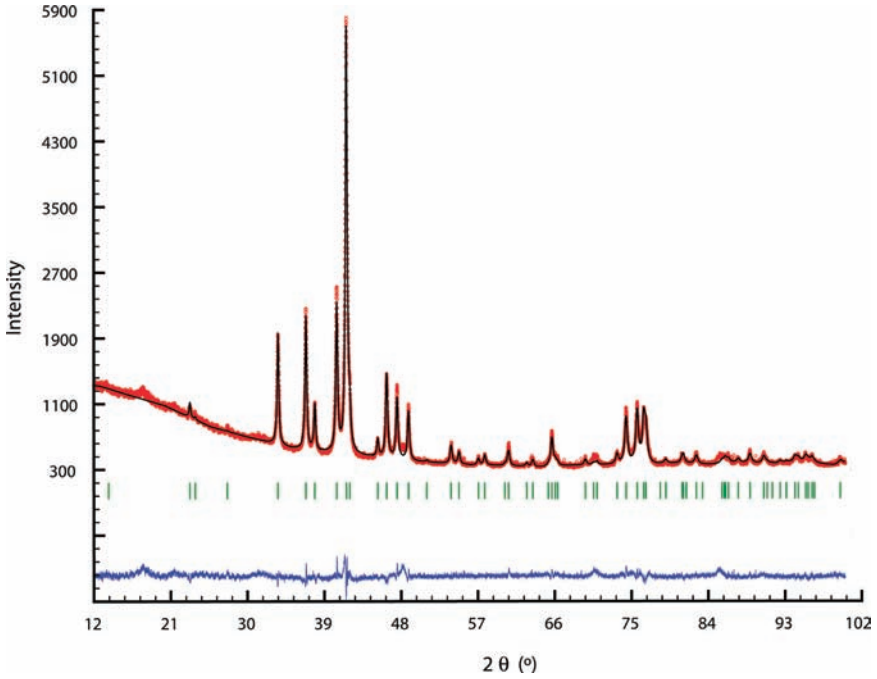

Figure 1. Rietveld refinement plot of the X-ray powder data of the $FeRh_6B_3$ phase showing measured and fitted intensities (top), the position of the Bragg peaks (middle), and the difference intensity curve (bottom).

Table 1. Results of the Rietveld Refinement for the Ternary Borides MRh_6B_3 (M = Fe, Co)

formula		$FeRh_6B_3$	$CoRh_6B_3$
fw [g/mol]		705.71	708.80
space group; Z		$P6_3mc$ (no. 186); 2	
structure refinement		RIETVELD, least-squares method	
profile function		pseudo-Voigt	
cell params	a [Å]	7.450(1)	7.443(2)
	c [Å]	4.748(1)	4.726(2)
	V [Å^3]	228.24(1)	226.78(2)
R_{Bragg}		0.082	0.142

components in the appropriate stoichiometric ratio on a water-cooled copper crucible under an argon atmosphere using a tungsten tip as the second electrode. The starting materials used for the synthesis were powders of cobalt (99.99%, Alfa Aesar), iron (99.99%, Alfa Aesar), rhodium (100% UMICORE AG & Co.KG, Hanau), and boron (amorphous 97%, ABCR; or crystalline pieces, 99.999%, Alfa Aesar). They were melted for about 15 s by an electric arc plasma with a direct current of 40 A until homogeneous melting occurred. Weight losses during the melting process were negligible. The obtained metallic lustrous regulus was mechanically cracked apart and pulverized for examination using a mortar and a pestle.

For the phase identification and the determination of lattice parameters at room temperature, X-ray powder methods were applied using a powder diffractometer [STOE Stadi P, transmission geometry; Cu $K_{\alpha 1}$ radiation (λ = 1.54059 Å), Ge monochromator, image plate detector, and silicon as standard].

We have also used Energy Dispersive X-ray analysis (EDX) with a high resolution, low energy SEM of the type LEO 1530 (Oberkochen, Germany) equipped with an EDX system of the type INCA (Oxford, England) to characterize the two metals present in each phase.

2.2. Crystal Structure Determination. A suitable single crystal could be isolated from the crushed regulus under an optical microscope for the sample composition $CoRh_6B_3$. The single crystal was fixed in a glass capillary, and the data were collected on a CCD single crystal diffractometer (Bruker SMART APEX) using graphite-monochromatized Mo K_α radiation (λ = 0.71073 Å). The X-ray intensities were corrected for absorption using a semiempirical procedure.[12] The crystal structure was solved using direct methods and refined by full-matrix least-squares refinement,[13] based on F^2, using anisotropic displacement parameters for all metals and an isotropic one for boron. [More details on the structure determination may be obtained from the Fachinformationszentrum Karlsruhe (e-mail address: crysdata@fiz-karlsruhe.de), D-76344 Eggenstein-Leopoldshafen, Germany, on quoting the CSD depository number CSD 422921 for $CoRh_6B_3$.] Rietveld refinements were also carried out for the MRh_6B_3 (M = Fe, Co) powder data, by full-matrix least-squares refinement implemented in the FULLPROF program.[14] The starting model for the Rietveld refinements evolved from the single crystal data.

2.3. Magnetic Measurements. Temperature-dependent susceptibility data on polycrystalline MRh_6B_3 (M = Fe, Co) samples were recorded with a SQUID magnetometer (MPMS-XLS, Quantum Design) in the temperature range 2.0−300 K for $FeRh_6B_3$ and 2.0−200 K for $CoRh_6B_3$ at applied fields up to B_0 = 5 T for both phases. The data were corrected for the sample holder (Teflon tubes).

2.4. Theoretical Methodology. Electronic structure calculations on $FeRh_6B_3$ and $CoRh_6B_3$ were performed using non-spin-polarized (nonmagnetic) and spin-polarized (magnetic) approaches. For a structural optimization concerning density functional theory, calculations with the Vienna *Ab-initio* Simulation Package (VASP),[15,16] including plane-waves basis sets and the projector-augmented wave (PAW)[17] method, have been performed. The kinetic energy cutoff for the plane waves was 500 eV, while exchange and correlation were treated in the generalized gradient approximation (GGA) using the exchange correlation functional from Perdew and Wang (PW91).[18] The interpolation formula according to Vosko, Wilk, and Nusair[19] was used to achieve a

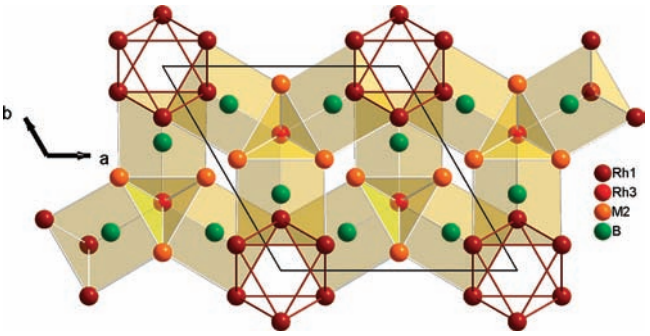

Figure 2. Projection of the crystal structure of the ternary boride $Co_{0.99(3)}Rh_{6.01(3)}B_3$ along [001]. Octahedral $(Rh1)_6$ cluster and the boron-centered trigonal prisms are highlighted. M2 = 2/3Rh2 + 1/3Co2.

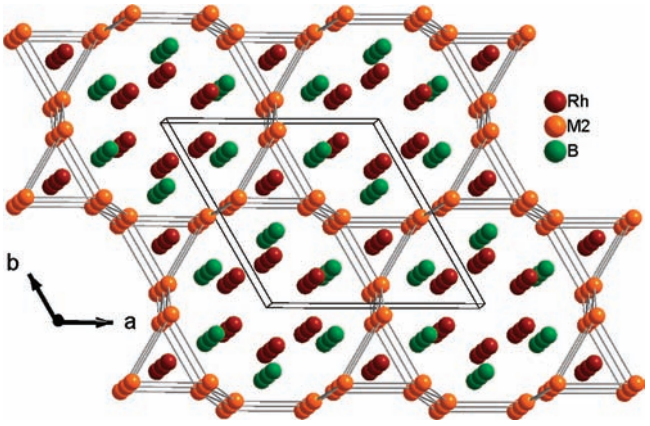

Figure 3. Projection nearly along [001] of the structure of $Co_{0.99(3)}Rh_{6.01(3)}B_3$, highlighting the three-dimensional network of interconnected $(M2)_3$ triangles (with M2 = 2/3Rh + 1/3Co).

higher accuracy with respect to the magnetic moments. The Brillouin zone integrations were performed using a 3 × 3 × 5 Monkhorst-Pack grid[20] resulting in a density of 900 *k* points × atoms. The interatomic forces were allowed to relax to values below 5×10^{-3} eV/Å and stresses below 1 kbar.

3. EXPERIMENTAL RESULTS AND DISCUSSION

3.1. Phase Analysis. The MRh_6B_3 (M = Fe, Co) samples were analyzed by Rietveld refinement of the X-ray powder diffraction data to determine the phases present and their lattice parameters. The structural model used for each refinement was created from the single-crystal data: the single-crystal refinement of $FeRh_6B_3$ was already reported,[9] whereas that of $CoRh_6B_3$ emanates from this work. All of the available peaks could be assigned to the Th_7Fe_3 structure type in each diffractogram (see for example that of $FeRh_6B_3$, Figure 1), thus each of the two products is a single phase. As expected when an element with a smaller atomic radius substitutes another with a larger one [in our case, one M (Fe or Co) substitutes one Rh in Rh_7B_3], the lattice parameters of the MRh_6B_3 phases (see Table 1) become smaller than those reported for the parent phase Rh_7B_3 (a = 7.47 Å, c = 4.78 Å). It has to be mentioned here that the single phase nature of these products and the presence of the two transition metals in each phase were also correctly reproduced by EDX analyses.

Table 2. Crystallographic and Single Crystal Structure Refinement Data of $CoRh_6B_3$

formula	$Co_{0.99(3)}Rh_{6.01(3)}B_3$
fw [g/mol]	708.82
$F(000)$	624
cryst size [mm^3]	0.08 × 0.05 × 0.02
θ range [deg]	$5.34 \le \theta \le 36.03$
hkl range	$-12 \le h \le 10$
	$-7 \le k \le 12$
	$-7 \le l \le 7$
no. reflns; R_{int}	2296; 0.0354
no. independent reflns	413
no. obsd. reflns $I > 2\sigma(I)$	397
Flack param; Friedel pairs	0.3(2); 183
no. params	21
space group; Z	$P6_3mc$ (no. 186); 2
cell params	
a [Å]	7.430(1)
c [Å]	4.7427(9)
V [$Å^3$]	226.74(6)
calcd density [g cm^{-3}]	10.38
abs. coeff μ [mm^{-1}]	24.67
GoF	1.13
R_1; wR_2 (all I)	0.0249; 0.0458
diff. peak/hole [e $Å^{-3}$]	1.42; −1.43

3.2. Structural Chemistry. In the crystal structure of the $FeRh_6B_3$ phase, an Fe/Rh site preference was observed.[9] In fact, as mentioned already in the Introduction, iron was found together with rhodium only on one of the available three rhodium sites. However, at higher iron contents (e.g., $Fe_{1.3}Rh_{5.7}B_3$ [10]) and in the ruthenium-containing phases (in $M_xRu_{7-x}B_3$ for instance with $x < 1$ and M = Cr, Mn, Fe, Co, Ni),[10,11] two of the available three sites are found to have a mixture of rhodium (or ruthenium) and the M element. The question at this point is, which of the two above-mentioned possibilities will be adopted in the $CoRh_6B_3$ structure? Because of the single phase nature of the $CoRh_6B_3$ product and the fact that it is a rhodium (not ruthenium)-containing phase having the same stoichiometry as $FeRh_6B_3$, its crystal structure is expected to be comparable to that of $FeRh_6B_3$. In other words, cobalt is expected (together with rhodium) at only one of the three crystallographic rhodium sites. Although the $CoRh_6B_3$ product is single phase, the Rh/Co mix-occupancy could not be refined freely using the Rietveld method. Satisfactory results were, however, obtained only after the corresponding amounts for cobalt and rhodium were imposed on the specified site. Therefore, single crystal refinement was necessary to confirm the composition and structure expected from this single phase product whose metal composition was also well reproduced by EDX analysis.

A single crystal was isolated from the $CoRh_6B_3$ product, and the structure could be solved and refined. The first refinement cycles provided three positions for rhodium, namely, two 6*c* sites (Rh1 and Rh2) and one 2*b* (Rh3). Boron was subsequently found on a 6*c* site, as expected. The 6*c* site occupied by Rh2 exhibited significantly larger displacement parameters than the two other rhodium sites. This indicates, indeed, a possible

dx.doi.org/10.1021/ic2013655 |*Inorg. Chem.* 2011, 50, 10303–10309

Table 3. Atomic Coordinates and Equivalent Displacement Parameters (U_{eq})[a] for $Co_{0.99(3)}Rh_{6.01(3)}B_3$

atom	Wyckoff position	occupancy	x	y	z	U_{eq}/Å^2
Rh1	6*c*	1.0	0.87469(4)	0.12531(4)	0.32598(6)	0.0069(2)
M2	6*c*	Rh2: 0.67(1)	0.54414(5)	0.45586(5)	0.00553(14)	0.0071(2)
		Co2: 0.33(1)				
Rh3	2*b*	1.0	1/3	2/3	0.0045(2)	0.0072(2)
B	6*c*	1.0	0.1868(7)	0.8132(7)	0.235(2)	0.010(2)

[a] U_{eq} is defined as 1/3 of the trace of the orthogonalized U_{ij} tensors. M2 = Rh2/Co2.

Table 4. Selected Interatomic Distances (Å) and Coordination in $Co_{0.99(3)}Rh_{6.01(3)}B_3$

Rh1	−B	1×	2.09(1)
	−B[b]	2×	2.166(6)
	−Rh1	2×	2.793(1)
	−M2	2×	2.782(1)
	−Rh3	1×	2.807(1)
	−M2[b]	2×	2.827(1)
	−Rh1[b]	4×	2.868(1)
M2[a]	−B	2×	2.175(7)
	−M2	2×	2.630(2)
	−B[b]	2×	2.641(2)
	−Rh3	1×	2.713(1)
	−M2[b]	2×	2.731(1)
	−Rh1	2×	2.782(1)
	−Rh1[b]	2×	2.827(1)
	−Rh3[b]	1×	2.843(2)
	−Rh3[b]	1×	2.852(2)
Rh3	−B	3×	2.178(1)
	−M2	3×	2.713(1)
	−Rh1	3×	2.808(1)
	−M2[b]	3×	2.843(2)
	−M2[b]	3×	2.852(2)
B1	−Rh1[b]	1×	2.09(1)
	−Rh1[b]	2×	2.166(6)
	−M2	2×	2.175(7)
	−Rh3	1×	2.178(1)

[a] M2 = Rh2/Co2. [b] Symmetry-related atoms.

site-sharing by rhodium and the electron-poorer cobalt. A mix-occupancy refinement using Rh/Co then improved the model significantly. After convergence of the refinement, the displacement parameters of the rhodium-rich M2 (Rh2/Co2) site were nearly similar to those of Rh1 and Rh3. As a consequence, very good residual values, R_1 = 0.0249 and wR_2 = 0.0458 for all 413 reflections and 21 parameters, were obtained. The occupancies of the M2 position were refined to 0.67(1)Rh2 + 0.33(1)Co2, leading to the composition $Co_{0.99(3)}Rh_{6.01(3)}B_3$, thus confirming and completing the EDX and X-ray powder diffraction results. Nevertheless, a mix-occupancy refinement was tried for the Rh1 and Rh3 sites, but no significant amount of Co could be refined in both cases. Consequently, the substitution of cobalt for rhodium takes place at the 6*c* site (occupied by Rh2) alone, as expected, and therefore the same site preference as in $FeRh_6B_3$ is observed. Just like in the case of $Fe_xRh_{7-x}B_3$ (x = 1, 1.3), it is very possible that other phases, besides the stoichiometric $CoRh_6B_3$ phase, with the general formula $Co_xRh_{7-x}B_3$ ($x \neq 1$), may be achieved. But we have restricted our investigations on the stoichiometric phases because their structures contain the magnetically active element at only one of the three available positions. This restriction is necessary because it allows for reliable discussion of the magnetic data and also facilitates the construction of structural models for electronic structure calculations.

There are two main characteristics of the crystal structures of MRh_6B_3 (M = Fe, Co): boron-centered trigonal prisms built up by rhodium and M2 (Rh2/M) atoms and the empty octahedral Rh_6 clusters (see Figure 2). M2 atoms build triangles, which are further connected to each other and engender a three-dimensional network (see Figure 3). This network is of particular interest because it contains a magnetically active transition metal and thus has the potential to induce long-range magnetic ordering in these phases. The distances in the network are 2.73 Å in the triangles and 2.63 Å between them in the Co-based phase and are respectively 2.71 Å and 2.62 Å in the Fe case.[9] Moreover, the remaining Rh−Rh, Rh−B, and M−B distances in $CoRh_6B_3$ are within expected ranges (see Table 4) and comparable not only with those of the $FeRh_6B_3$ phase but also with those found for similar phases, for example, in $Co_{0.5}Ru_{6.5}B_3$.[12]

All relevant crystallographic data and experimental details of the data collection for $CoRh_6B_3$ are listed in Table 2. Table 3 contains the atomic coordinates and the equivalent displacement parameters, while Table 4 summarizes the selected interatomic distances.

3.3. Magnetic Properties. The magnetic data of the compounds $FeRh_6B_3$ and $CoRh_6B_3$ were recorded with a SQUID magnetometer in the temperature range 2−300 K and applied fields up to B_0 = 5 T. The presentation of the magnetic data follows the recommendation of Hatscher et al. (SI units).[21] According to the variation of the atomic magnetic dipole moment (μ_a) versus temperature (see Figure 4), both phases exhibit spontaneous magnetization below $T_C \approx 240$ K for $FeRh_6B_3$ and $T_C \approx 150$ K for $CoRh_6B_3$ (T_C is deduced from the intersection of a linear fit of the steepest part of the magnetization curve with the temperature axis at low magnetic field). The paramagnetic Curie−Weiss region is observed for $T >$ 300 K in the Fe case, whereas in the Co case it is found already at $T >$ 200 K. A positive and high paramagnetic Weiss temperature (θ) could also be determined to be 238 and 94 K, for $FeRh_6B_3$ and $CoRh_6B_3$, respectively, indicating strong ferromagnetic exchange interactions in both phases. The two compounds therefore show ferromagnetic ordering below their respective Curie temperatures. However, the iron-based phase clearly has much higher ferromagnetic characteristics than the cobalt-based one. This indicates that the overall magnetic behavior of these phases strongly depends on the local magnetic moment on the magnetically active element and its ability to induce a fictive

dx.doi.org/10.1021/ic2013655 |Inorg. Chem. 2011, 50, 10303–10309

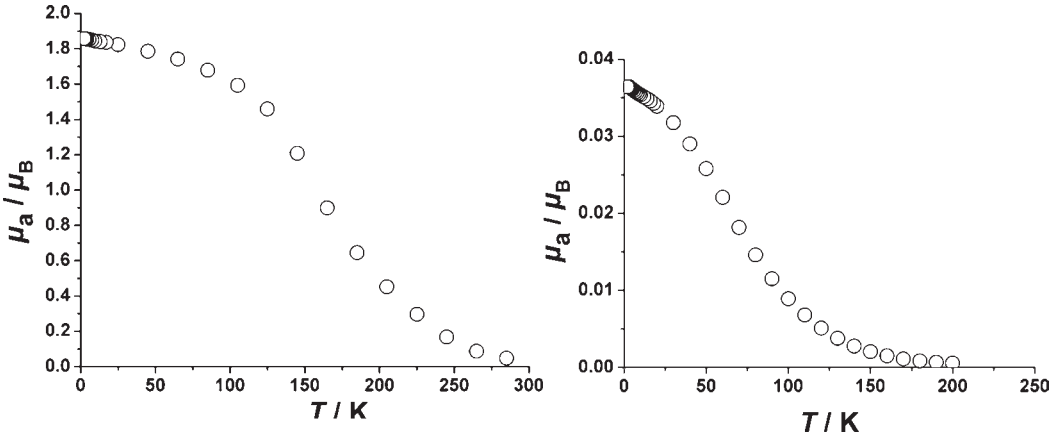

Figure 4. Variation of the atomic magnetic dipole moment (μ_a) per formula MRh_6B_3 as a function of the temperature at an applied magnetic field B_0 = 0.1 T for $FeRh_6B_3$ (left) and B_0 = 0.01 T for $CoRh_6B_3$ (right).

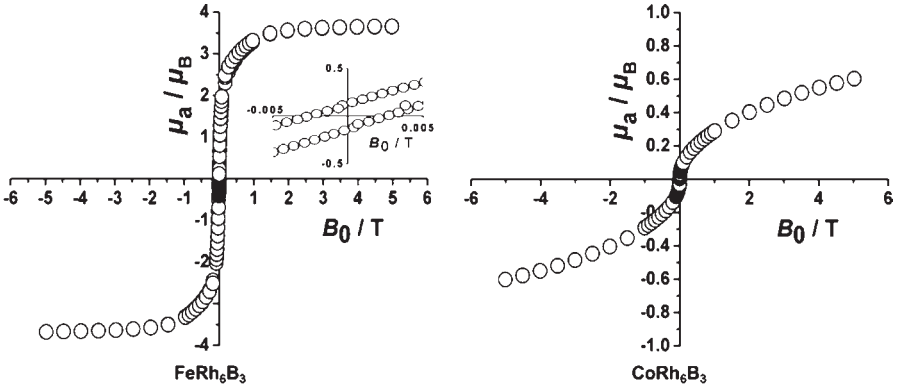

Figure 5. Hysteresis loop of $FeRh_6B_3$ at 5 K (left). A part of this loop has been enlarged, and it displays the remnant magnetization and the coercive field (inset). On the right-hand side is the hysteresis loop of $CoRh_6B_3$ at 5 K.

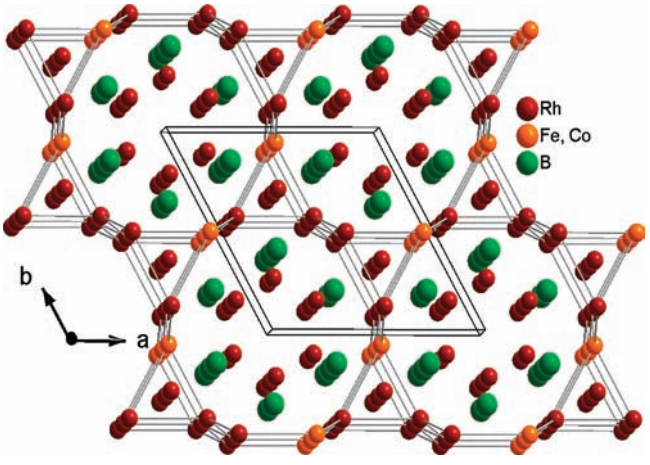

Figure 6. Projection nearly along [001] of the triclinic structural model of MRh_6B_3 (M = Fe, Co) highlighting the three-dimensional network of interconnected triangles shown in Figure 2 but with distinct M and Rh sites. In this model, there are no direct M−M interactions.

moment on the nearby rhodium site. This assumption was even quantified in the theoretical section using density functional theory calculations (see section 4.3).

Hysteresis loops were also recorded at 5 K within a magnetic field range of ±5 T (see Figure 5). A saturation magnetic moment was reached only in the $FeRh_6B_3$ phase with a value of μ_a^S (exptl) = 3.60 μ_B at an applied field B_0 = 3 T, whereas in the case of $CoRh_6B_3$, μ_a remains unsaturated, reaching a value of about 0.64 μ_B at 5 T, the highest field applied. According to the determined values of the coercivity (H_c = 2069 A/m for $FeRh_6B_3$ and H_c = 1691 A/m for $CoRh_6B_3$), the two compounds may be classified as semihard ferromagnets.

These two phases are the first ferromagnetic borides adopting the Th_7Fe_3 structure type. The presence of 1/3 of Co (or Fe) in a three-dimensional network of Rh/Co (or Rh/Fe) atoms seems to be the driving force behind this magnetic ordering. As already mentioned above, the distances in the network are 2.73 Å in $(Rh/Co)_3$ triangles and 2.63 Å between them in the Co case and are respectively 2.71 Å and 2.62 Å in the Rh/Fe network. Although these distances are somewhat larger than those found in the ferromagnetic iron and cobalt elements, they remain smaller than those found in other transition metal boride phases which also show ferromagnetic ordering: For example, in the ferromagnetic phases of the $Sc_2FeRu_{5-n}Rh_nB_2$ (n = 3−5) and $Ti_2FeRu_{5-n}Rh_nB_2$ (n = 1−5) series, the smallest Fe−Fe distances are ca. 3.0 Å.[22] Furthermore, using DFT calculations, it was found in the $Sc_2FeRu_{5-n}Rh_nB_2$ series that the ferromagnetic interactions were mediated by rhodium atoms,[23] a scenario

dx.doi.org/10.1021/ic2013655 |Inorg. Chem. 2011, 50, 10303–10309

Table 5. Calculated (calcd) and Experimental (exptl) Lattice Parameters (a, c), Saturated Magnetic Moments (μ_a^S), and Local Magnetic Moments (μ_a^L) for MRh_6B_3 (M = Fe, Co) Phases

MRh_6B_3		a [Å]	c [Å]	V [Å^3]	μ_a^S [μ_B]	μ_a^L (M)[μ_B]	μ_a^L (Rh)[μ_B]
M = Fe	calcd	7.498	4.796	233.51	4.02	2.77	0.22
	exptl	7.450(1)	4.748(1)	228.24(1)	3.60		
M = Co	calcd.	7.500	4.751	231.44	2.75	1.50	0.22
	exptl	7.443(2)	4.726(2)	226.78(1)			

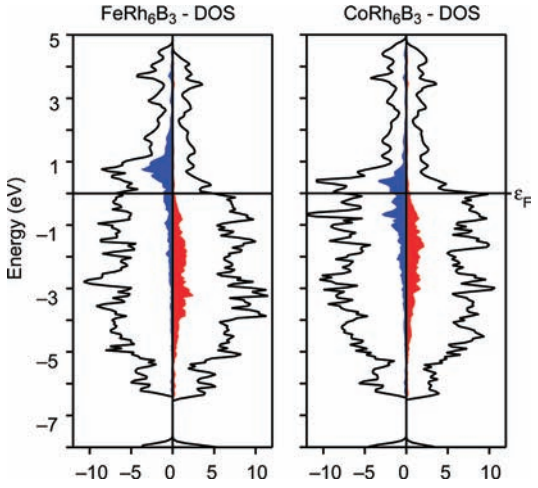

Figure 7. Total and colored projected DOS (for Fe or Co) in the ferromagnetic phases $FeRh_6B_3$ (left) and $CoRh_6B_3$ (right). All curves have been shifted so that the Fermi level lies at energy zero. The α- and β-spin densities (for Fe or Co) are in red and blue colors, respectively.

which is also expected in the herein reported compounds in particular because the above-mentioned network is dominated by rhodium atoms.

In order to gain more insight into the magnetic ordering observed in these two phases, theoretical calculations of the DFT type were applied, the results of which are discussed in the following section.

4. RESULTS AND DISCUSSION OF THE DFT CALCULATIONS

We have performed first-principles calculations of the density functional type on the two MRh_6B_3 (M = Fe, Co) phases to first assess the theoretical crystallographic parameters and second study the magnetic properties.

4.1. Modeling the Rh/M Site Preference: Supercell approach versus Triclinic Symmetry. As demonstrated above already, a Rh/M site preference is observed in the crystal structures of the MRh_6B_3 (M = Fe, Co) phases: One of the two available crystallographic 6*c* Rh positions has a mix occupation of one-third M and two-thirds Rh. There are innumerable possibilities to describe the resulting statistical unit cell [space group $P6_3mc$ (no. 186)]. To stay within a reasonable time scheme for computation, we accomplished DFT calculations of a 3-fold unit cell (supercell approach), by tripling the *c* axis but preserving the above-mentioned space group's symmetry. Within this symmetry, iron triangles appear (see Supporting Information Figures S1 and S2), which at first glance, seem to be the origin for an increased local magnetic ordering through direct coupling of the M atoms. In this model, the long-range magnetic ordering may occur through indirect coupling of the M_3 triangles by the nearby rhodium atoms.

Another way to look at statistical distributions is to do calculations based on a triclinic cell, through symmetry breaking. This makes it possible to stay within the small unit cell and thus speeds the calculations. The two iron atoms per cell can then be distributed on the available six positions which originate from the 6*c* symmetry breaking. Consequently, 15 possibilities to distribute two iron atoms in one unit cell exist. One of these distributions (Figure 6) was lowest in energy and also close (in energy) to the 3-fold supercell case. In this model, there is no direct coupling between iron atoms, in strong contrast to the supercell model where M_3 triangles exist.

By comparing the energies in both cases as well as the simulated X-ray diffraction patterns with the measured one (see Supporting Information Figure S3), we could eliminate the supercell configuration. Therefore, no direct coupling between the iron moments exists; thus only indirect coupling through the neighboring rhodium atoms is expected.

4.2. Crystallographic Parameters. The results obtained by first-principles VASP calculations of the crystallographic parameters of the $FeRh_6B_3$ phase will be first discussed, followed by those of the cobalt phase. In fact, the lattice parameters and the bonding situation in $FeRh_6B_3$ could be well reproduced by the triclinic model after relaxation of the structure: The GGA-calculated ground state lattice parameters, $a \approx b = 7.498$ Å and $c = 4.796$ Å (triclinic symmetry), are slightly higher than the experimental values ($a = 7.450$ Å, $c = 4.748$ Å, hexagonal symmetry), which means a typical GGA overestimation of only 0.6% and 1% for *a* and *c*, respectively. This slight overestimation is further reflected in the bonding situation of this phase. For example, the bonds between iron and the surrounding rhodium atoms are 2.73 Å and 2.64 Å, which are just slightly larger than the experimentally observed values (2.71 Å and 2.62 Å, respectively)[8] in the M2(2/3Rh+1/3Fe) network (see Figure 6).

The results obtained for the $CoRh_6B_3$ phase were also very close to the experimental ones (with the typical GGA overestimation) and are reported in Table 5. Furthermore, the same unit cell volume trend is observed in both cases (experiment and theory): The cell volume of the Fe-based phase is significantly larger (by 1.46 Å^3 in the experiment and by 2.07 Å^3 in theory) than that of the Co-based one (see Table 5). Taking into account that Fe and Co have nearly the same atomic radius, size factors play only a negligible role in this behavior; therefore electronic factors are mainly responsible and also justify the good prediction of the volume trend.

4.3. Magnetic Ordering and Quantities. To probe the magnetic ordering in these phases, ferromagnetic (spin polarized) calculations were applied for the MRh_6B_3 (M = Fe, Co) phases. Figure 7 is a plot of the DOS diagrams for the ferromagnetic compounds $FeRh_6B_3$ and $CoRh_6B_3$ calculated using VASP. It shows two typical conductors and

a spin split, which is dominated by iron (or cobalt), whose α-spin densities, shown to the right, gather almost all states below the Fermi level. The cobalt compound's states are more contracted, and thus they have a minor spin split, indicating a lower magnetic moment than that of the iron compound. Indeed, the calculated magnetic saturation moment for $FeRh_6B_3$ (μ_a^S = 4.02 μ_B) is much higher than that of $CoRh_6B_3$ (μ_a^S = 2.75 μ_B). Experimentally, the magnetic moment was found to be much higher in $FeRh_6B_3$ than in $CoRh_6B_3$ (see Experimental Results, section 3.3), and the experimental saturation moment found for the iron-based phase (μ_a^S (exptl) = 3.60 μ_B) is just slightly smaller than the predicted value (see above). The local moments on the magnetically active iron and cobalt are 2.77 μ_B and 1.50 μ_B, respectively. To account for the total magnetic moment in each phase, a small contribution originates from the rhodium atoms (average 0.22 μ_B in both phases, see Table 5). These calculations therefore confirm and even improve the experimental results: $FeRh_6B_3$ and $CoRh_6B_3$ are, indeed, the first ferromagnetic boride phases adopting the Th_7Fe_3 structure type. Furthermore, the DOS calculations presented above have predicted metallic behaviors for the two phases, as expected for these metal-rich phases whose crystals show metallic luster. Consequently, they are itinerant ferromagnets.

5. CONCLUSIONS

The first itinerant ferromagnetic borides of the Th_7Fe_3 structure type, MRh_6B_3 (M = Fe, Co), have been successfully synthesized as single phase products. The magnetically active M atom is found preferentially at one of three rhodium sites, building a three-dimensional network of interconnected $(Rh/M)_3$ triangles. Magnetic properties investigations show that both phases order ferromagnetically below Curie temperatures of 240 K (for $FeRh_6B_3$) and 150 K (for $CoRh_6B_3$). The recorded hysteresis loops show a saturation magnetization in the iron case (with a saturation moment of 3.60 μ_B), whereas in the cobalt case no saturation could be achieved up to 5 T. DFT calculations correctly reproduce the lattice parameters in both cases and predict metallic behaviors, as expected from these metal-rich phases. The ferromagnetic ordering in both phases and the saturation magnetization in the iron case were also correctly predicted.

■ ASSOCIATED CONTENT

Supporting Information. Hypothetical supercells of $FeRh_6B_3$ and a comparison between measured and simulated diffractograms of $FeRh_6B_3$. This material is available free of charge via the Internet at http://pubs.acs.org.

■ AUTHOR INFORMATION

Corresponding Author
*E-mail: boniface.fokwa@ac.rwth-aachen.de.

■ ACKNOWLEDGMENT

The authors wish to acknowledge Deutsche Forschungsgemeinschaft (DFG) for financial support, Klaus Kruse for technical support during the X-ray experiments, and Resi Zaunbrecher (IPC, RWTH Aachen) for the EDX analyses. B.P.T.F. is also grateful to the DFG for awarding him the Heisenberg fellowship.

■ REFERENCES

(1) (a) Brazhkin, V. V.; Lyapin, A. G.; Hemley, R. J. *Phil. Magn.* **2002**, *82*, 231. (b) Fokwa, B. P. T. *Eur. J. Inorg. Chem.* **2010**, 3075.
(2) Florio, J. V.; Baenziger, N. C.; Rundle, R. E. *Acta Crystallogr.* **1956**, *9*, 367.
(3) Malik, S. K.; Wallace, W. E.; Takeshita, T. *Solid State Commun.* **1978**, *28*, 359.
(4) Sengupta, K.; Iyer, K. K.; Sampathkumaran, E. V. *Solid State Commun.* **2006**, *139*, 351.
(5) Talik, E.; Klimczak, M.; Troc, R.; Kusz, J.; Hofmeister, W.; Winiarski, A. *J. Alloys Compd.* **2008**, *460*, 1.
(6) (a) Matthias, B. T.; Geballe, T. H.; Compton, V. B. *Rev. Mod. Phys.* **1963**, *35*, 1. (b) Fang, L.; Yang, H.; Zhu, X.; Mu, G.; Wang, Z.-S.; Shan, L.; Ren, C.; Wen, H.-H. *Phys. Rev. B* **2009**, *79*, 144509. (c) Kase, N.; Akimitsu, J. *J. Phys. Soc. Jpn.* **2009**, *78*, 044710.
(7) Kuz'ma, Y. B.; Chepiga, M. V. *Inorg. Mater.* **1973**, *9*, 1505.
(8) Chepiga, M. V. *L'viv. Derzh. Univ. (ser. Khim.)* **1972**, 14.
(9) Fokwa, B. P. T.; Dronskowski, R. *Z. Anorg. Allg. Chem.* **2005**, *631*, 2478.
(10) Fokwa, B. P. T.; Dronskowski, R. *J. Alloys Compd.* **2007**, *428*, 84.
(11) Misse, P. R. N.; Fokwa, B. P. T. *Z. Anorg. Allg. Chem.* **2010**, 636.
(12) Sheldrick, G. M. *SADABS*; University of Göttingen: Göttingen, Germany, 2001.
(13) Sheldrick, G. M. *Acta Crystallogr.* **2008**, *A64*, 112.
(14) Rodriguez-Carvajal, J. *FULLPROF*, Version July 2004, ILL (unpublished).
(15) Kresse, G.; Hafner, J. *Phys. Rev. B* **1993**, *47*, 558. *Phys. Rev. B* **1994**, *49*, 14251.
(16) Kresse, G.; Furthmüller, J. *Comput. Mater. Sci.* **1996**, *6*, 15. *Phys. Rev. B* **1996**, *55*, 11169.
(17) Blöchl, P. E. *Phys. Rev. B* **1994**, *50*, 17953.
(18) Perdew, J. P. *Electronic Structure of Solids*; Ziesche, P., Eschrig, H., Eds.; Akademie Verlag: Berlin, 1991.
(19) Vosko, S. H.; Wilk, L.; Nusair, M. *Can. J. Phys.* **1980**, *58*, 1200.
(20) Monkhorst, H. J.; Pack, J. D. *Phys. Rev. B* **1976**, *13*, 5188.
(21) Hatscher, S. T.; Schilder, H.; Lueken, H.; Urland, W. *Pure Appl. Chem.* **2005**, *77*, 497.
(22) (a) Fokwa, B. P. T.; Lueken, H.; Dronskowski, R. *Chem.—Eur. J.* **2007**, *13*, 6040.(b) Fokwa, B. P. T.; Lueken, H.; Dronskowski, R. *Eur. J. Inorg. Chem.* **2011**, DOI: 10.1002/ejic.201100315.
(23) Samolyuk, G.; Fokwa, B. P. T.; Dronskowski, R.; Miller, G. J. *Phys. Rev. B* **2007**, *76*, 094404.